

Adaptive multi-stable stochastic resonance assisted by neural network and physical supervision

Xucan Li(李栩灿), Deming Nie(聂德明), Ming Xu(徐明), and Kai Zhang(张凯)

Citation: Chin. Phys. B, 2025, 34 (**5**): 050203. DOI: 10.1088/1674-1056/adbd28
Journal homepage: http://cpb.iphy.ac.cn; http://iopscience.iop.org/cpb

What follows is a list of articles you may be interested in

Dynamic properties of rumor propagation model induced by Lévy noise on social networks

Ying Jing(景颖), Youguo Wang(王友国), Qiqing Zhai(翟其清), and Xianli Sun(孙先莉)
Chin. Phys. B, 2024, 33 (**9**): 090203. DOI: 10.1088/1674-1056/ad58c5

Performance enhancement of a viscoelastic bistable energy harvester using time-delayed feedback control

Mei-Ling Huang(黄美玲), Yong-Ge Yang(杨勇歌), and Yang Liu(刘洋)
Chin. Phys. B, 2024, 33 (**6**): 060203. DOI: 10.1088/1674-1056/ad3b89

Research and application of composite stochastic resonance in enhancement detection

Rui Gao(高蕊), Shangbin Jiao(焦尚彬), and Qiongjie Xue(薛琼婕)
Chin. Phys. B, 2024, 33 (**1**): 010203. DOI: 10.1088/1674-1056/ad01a8

Weak signal detection method based on novel composite multistable stochastic resonance

Shangbin Jiao(焦尚彬), Rui Gao(高蕊), Qiongjie Xue(薛琼婕), and Jiaqiang Shi(史佳强)
Chin. Phys. B, 2023, 32 (**5**): 050202. DOI: 10.1088/1674-1056/aca4bd

Inverse stochastic resonance in modular neural network with synaptic plasticity

Yong-Tao Yu(于永涛) and Xiao-Li Yang(杨晓丽)
Chin. Phys. B, 2023, 32 (**3**): 030201. DOI: 10.1088/1674-1056/aca602

Adaptive multi-stable stochastic resonance assisted by neural network and physical supervision

Xucan Li(李栩灿), Deming Nie(聂德明), Ming Xu(徐明)†, and Kai Zhang(张凯)

College of Metrology Measurement and Instrument, China Jiliang University, Hangzhou 310018, *China*

(Received 23 December 2024; revised manuscript received 27 January 2025; accepted manuscript online 6 March 2025)

Stochastic resonance can utilize the energy of noise to enhance weak frequency characteristic. This paper proposes an adaptive multi-stable stochastic resonance method assisted by the neural network (NN) and physics supervision (directly numerical simulation of the physical system). Different from traditional adaptive algorithm, the evaluation of the objective function (i.e., fitness function) in iteration process of adaptive algorithm is through a trained neural network instead of the numerical simulation. It will bring a dramatically reduction in computation time. Considering predictive bias from the neural network, a secondary correction procedure is introduced to the reevaluate the top performers and then resort them in iteration process through physics supervision. Though it may increase the computing cost, the accuracy will be enhanced. Two examples are given to illustrate the proposed method. For a classical multi-stable stochastic resonance system, the results show that the proposed method not only amplifies weak signals effectively but also significantly reduces computing time. For the detection of weak signal from outer ring in bearings, by introducing a variable scale coefficient, the proposed method can also give a satisfactory result, and the characteristic frequency of the fault signal can be extracted correctly.

Keywords: stochastic resonance, multi-stable, physical supervision, neural network, fault diagnosis

PACS: 02.60.Pn, 02.60.Cb, 05.40.–a, 05.45.–a, 07.05.Mh

DOI: 10.1088/1674-1056/adbd28 **CSTR:** 32038.14.CPB.adbd28

1. Introduction

Stochastic resonance (SR) represents a rather counterintuitive phenomenon. Typically, in engineering applications, noise is conventionally regarded as having adverse or harmful effects. However, under specific circumstances, SR has the remarkable ability to generate positive and beneficial outcomes from noise.[1] Within nonlinear systems, SR brings about advantageous effects via mechanisms such as noise-enhanced stability,[2] noise-induced phase transitions,[3] resonance activation,[4] and stochastic resonance.[5] After decades of continuous development and in-depth research, SR has been extensively investigated and applied across a diverse range of fields, including physics,[6] biological neuroscience,[7,8] chemical reactions,[9,10] and mechanical engineering.[11] The theory and application of SR remain highly active and prominent research topics, attracting significant attention and efforts from the scientific community.

In recent years, the research on SR has witnessed a remarkable transformation from mono-stable systems to multi-stable systems. This shift has led to the manifestation of more elaborate and diverse dynamic characteristics, accompanied by substantial enhancements in performance. Dykman *et al.*[12] delved into SR within over-damped mono-stable systems by leveraging linear response theory. Lindner *et al.*[13] probed into the aspects of coherence and SR in bi-stable systems. Liu *et al.*[14] adopted the signal-to-noise ratio (SNR) as an index for signal quality and explored the phenomenon of symmetric tri-stable SR under Lévy distributed noise. Liao *et al.*[15] pioneered the introduction of a logic stochastic resonance (LSR) system predicated on quad-stable nonlinearity with the aim of augmenting noise robustness and output quality. The outcomes of their study indicated that the quad-stable LSR could endure a maximum noise intensity that surpassed that of the tri-stable LSR. Gong *et al.*[16] scrutinized the SR in a five-stable configuration energy harvesting system, thereby augmenting the energy harvesting performance in random rotational environments. These research findings undeniably confirm that multi-stable systems have obvious advantages in signal amplification and noise immunity, thus promoting the development of SR theory in complex and intricate environments.

The parameters of the potential function in a nonlinear system can influence the structure of the potential function and consequently the output of SR. Simultaneously, noise intensity also impacts the output of SR. However, it is challenging to select a set of parameters that match the noise intensity. The adaptive stochastic resonance (ASR) theory[17] addresses the issue of matching the parameters of a nonlinear system with the input signal and noise intensity. ASR is founded on a series of intelligent optimization algorithms and adaptively adjusts system parameters to enhance signal detection capability. Liu *et al.*[18] proposed a method to adjust SR for different operating conditions by optimizing system parameters using the artificial fish swarm algorithm. Lei *et al.*[19] also proposed

†Corresponding author. E-mail: xuming@cjlu.edu.cn

© 2025 Chinese Physical Society and IOP Publishing Ltd. All rights, including for text and data mining, AI training, and similar technologies, are reserved.

a similar approach. Li *et al.*[20] introduced an ASR method based on a sliding window, which has been successfully applied in the gearbox fault diagnosis of the finishing mill for hot strip steel.

In the field of bearing fault detection, SR has demonstrated significant potential, particularly in enhancing weak fault features in low SNR environments. Hu *et al.*[21] applied an SR model to detect early rotor rubbing and friction faults, validating the reliability of the method. Guo *et al.*[22] proposed an improved cascading SR for detecting weak fault signals in bearings, effectively enhancing multi-frequency signals by segmenting the input signals. Li *et al.*[23] introduced a novel ASR method based on coupled bi-stable systems, further improving the detection performance of weak signals. Jin *et al.*[24,25] optimized multi-stable SR parameters using quantum particle swarm optimization and achieved promising results in bearing fault detection. Nevertheless, in practical bearing fault detection, high sampling frequencies are often employed to approximate real data, resulting in a large number of signal samples. Computing the response of each sample point using numerical computation methods can be time-consuming.

Although existing ASR methods have shown great potential in weak signal detection, they still exhibit certain limitations. For instance, SR methods utilizing genetic algorithms often face slow convergence rates, while particle swarm optimization struggles with balancing the global and local optima effectively. Traditional ASR methods typically require numerical computations for each sampling point, which leads to a significant increase in computational complexity, especially with high sampling frequencies. To tackle the complexity of numerical computation, this paper proposes an adaptive multi-stable stochastic resonance based on a neural network and physics supervision (ASR-PSNN). The evaluation of the fitness in iteration process of adaptive algorithm is done by the PSNN model instead of the complex numerical calculations.

The remainder of this paper is organized as follows: Section 2 introduces the principles of multi-stable stochastic resonance (MSR), which forms the foundation for subsequent research based on the structure of the potential function. Section 3 presents a novel ASR algorithm by using a neural network and physics supervision. Section 4 presents the results of weak signals detection using the proposed method. Finally, Section 5 concludes the paper.

2. Multi-stable stochastic resonance

Consider a first-order overdamped SR system, the motion equation is expressed as follows:

$$\begin{cases} \dot{x} = -U'(x) + A_0 \sin(2\pi f_0 t) + \sqrt{2D}\xi(t), \\ \langle \xi(t) \rangle = 0, \langle \xi(t), \langle \xi(0) \rangle \rangle = \delta(t), \end{cases} \tag{1}$$

where A_0 is the amplitude of the input signal, f_0 is the frequency of the input signal, $\xi(t)$ is unit Gaussian white noise, $2D$ is the noise intensity and $U(x)$ is the potential function of the system. The symbol "$'$" denotes the differential with respect to x and "$\cdot$" is the differential with respect to time t. The form of the potential function used in the paper is shown in Eq. (2),[25,26] where $U(x)$ has four stable points x_1, x_2, x_3, x_4, and three unstable points x_0, x_5, x_6. The potential function is illustrated in Fig. 1.

$$U(x) = -\frac{1}{2}ax^2 + \frac{1}{4}bx^4 - \frac{1}{6}cx^6 + \frac{1}{8}dx^8. \tag{2}$$

Substituting the potential function into Eq. (1), we obtain the following form

$$\dot{x} = ax - bx^3 + cx^5 - dx^7 + A\sin(2\pi ft) + \sqrt{2D}\xi(t). \tag{3}$$

By adjusting the parameters a, b, c, d in the potential function, different stable states can be generated. The potential function may form a quad-stable status with different potential well depths, as shown in Fig. 2(a). Further adjustment of the potential function parameters can transform the system into a bi-stable status as shown in Fig. 2(b). Therefore, in the optimizing SR procedure, the optimal SR system is seleced from sets of various quad-stable and bi-stable situations.

By rewriting Eq. (3) in the following form, the SR model for a small parameter input signal can be expressed as

$$\begin{aligned} \frac{\mathrm{d}x}{\mathrm{d}t} &= a_0 x - b_0 x^3 + c_0 x^5 - d_0 x^7 \\ &\quad + A_0 \sin(2\pi f_0 t) + \sqrt{2D_0}\xi(t), \end{aligned} \tag{4}$$

where a_0, b_0, c_0, d_0 are the system parameters of the potential function, A_0 is the amplitude of the input signal, f_0 is the frequency of the input signal, $\sqrt{2D_0}\xi(t)$ represents the Gaussian white noise term with noise intensity $2D_0$.

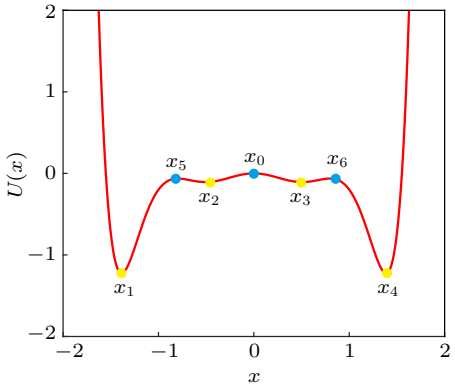


Fig. 1. A schematic diagram of the potential function $U(x)$.

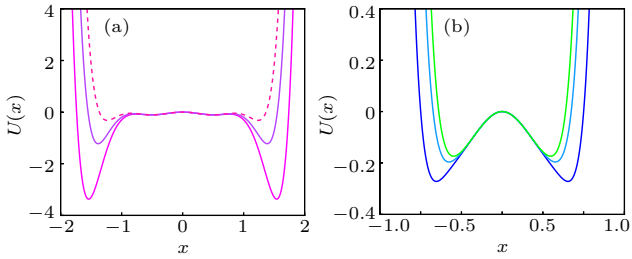


Fig. 2. Potential function curves under various system parameters: (a) the quad-stable status, (b) the bi-stable status.

When the input signal is a high-frequency signal ($f \gg 1$), the SR system is shown as follows:

$$\frac{\mathrm{d}x}{\mathrm{d}t} = ax - bx^3 + cx^5 - dx^7 + A\sin(2\pi ft) + \sqrt{2D}\xi(t), \quad (5)$$

the parameters in Eq. (5) are much larger than those in Eq. (4). Classical SR theory, based on the adiabatic approximation theory[27,28] and linear response theory derivations,[29] is suitable for cases where the input signal consists of small parameters. If a high-frequency signal is directly input into a nonlinear system, the theory suggests that SR cannot be obtained. Therefore, parameter scaling transformation is required to satisfy small parameter condition. The transformation is introduced as follows:[30]

$$x(t) = z(\tau), \quad \tau = mt, \quad (6)$$

where m is the scaling factor. Substituting Eq. (6) into Eq. (5), we obtain

$$\frac{\mathrm{d}z}{\mathrm{d}\tau} = \frac{1}{m}\left(ax - bx^3 + cx^5 - dx^7 + A\sin\left(2\pi\frac{f}{m}\tau\right)\right) + \sqrt{\frac{2D}{m}}\xi(\tau). \quad (7)$$

Denote $a_1 = a/m$, $b_1 = b/m$, $c_1 = c/m$, $d_1 = d/m$, $f_1 = f/m$, substituting these into Eq. (7), we get

$$\frac{\mathrm{d}z}{\mathrm{d}\tau} = a_1 x - b_1 x^3 + c_1 x^5 - d_1 x^7 + \frac{A}{m}\sin(2\pi f_1 \tau) + \sqrt{\frac{2D}{m}}\xi(\tau). \quad (8)$$

Here, the large parameters a, b, c, d have been transformed into small parameters a_1, b_1, c_1, d_1. However, the amplitude of the signal A and the noise intensity D have been reduced, so they need to be multiplied by m to restore their original level. After rearranging, we get

$$\frac{\mathrm{d}z}{\mathrm{d}\tau} = a_1 x - b_1 x^3 + c_1 x^5 - d_1 x^7 + A\sin(2\pi f_1 \tau) + \sqrt{2D}\xi(\tau). \quad (9)$$

At this point, all terms in Eq. (9) meet the small parameter conditions for SR. To achieve stochastic resonance with large parameters, all terms need to be unified as large parameters, which requires amplifying the input signal amplitude and noise intensity by a factor of m to match all parameters

$$\frac{\mathrm{d}x}{\mathrm{d}t} = ax - bx^3 + cx^5 - dx^7 + mA\sin(2\pi ft) + \sqrt{2Dm}\xi(t). \quad (10)$$

3. Adaptive MSR using neural network and physical supervision

In this section, we propose an ASR procedure that combines physical supervision and neural network (ASR-PSNN). This method modifies the traditional genetic algorithm (GA) to optimize the improved signal-to-noise ratio (ISNR),[24] and alter the fitness value in GA process by introducing a neural network and physical supervision, which enhances computational efficiency and keeps the optimizing accuracy.

3.1. Selection of GA operators

GA is a classical intelligent optimization algorithm based on the principle of natural selection,[31] capable of optimizing multiple parameters.[32] It has been widely applied as an effective optimization tool to solve various engineering problems.[33]

There are multiple selection methods for genetic operators in GA. In this paper, binary encoding is adopted. Single-point crossover and bit mutation are applied to chromosomes composed of binary-encoded genes, and the tournament method is used for individual selection, as shown in Fig. 3. In GA, binary encoding is performed for n parameters, and the length l of each segment of the code needs to be determined based on the parameter's range of values and the required precision.[34] Suppose the range of a parameter is $[m_1, m_2]$, then the length of each segment is determined as follows:

$$l = m_2 - m_1, \quad 2^{n_i - 1} < l/p < 2^{n_i}, \quad (11)$$

where l is the length of the parameter's value range, p is the required precision of the parameter, and n_i is the length of the sub-encoded string. Based on this, the length of each sub-encoded string can be determined.

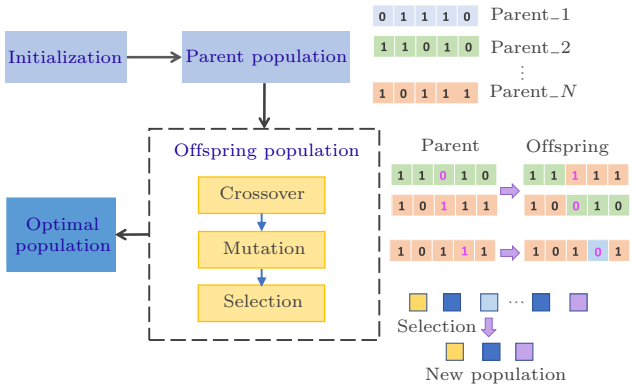


Fig. 3. Schematic diagram of the GA with operator selection.

3.2. Stochastic resonance measurement index

Parameters a, b, c, d of the potential function in MSR system (3) or (10) are optimized using GA, where the fitness function is selected as ISNR and its expression is

$$\begin{cases} \mathrm{ISNR} = 10\log_{10}\left(\dfrac{P_\mathrm{S}(f)}{P_\mathrm{N}(f) - P_\mathrm{S}(f)}\right), \\ P_\mathrm{S}(f) = \left|X(k)^2\right|, \\ P_\mathrm{N}(f) = \sum_i^j\left(\left|X(i)^2\right|\right), \quad 1 \le i < k; k < j, \end{cases} \quad (12)$$

where $P_S(f)$ represents the power at the characteristic frequency f, and $P_N(f)$ is the total power of the local background noise near frequency f, $X(k)$ is the Fourier transform of the input signal's time series, and i and j define the length of the signal used for calculating the local total power.

3.3. Neural network (NN) prediction and physical supervision

The main procedure of ASR-PSNN is similar to the traditional ASR process, as shown in Fig. 4. One key difference is that the fitness function evaluation is replaced by the NN model instead of using the fourth-order Runge–Kutta method (RK4). First, within the specified range $[l_1, l_2]$ for each dimension of the potential function's parameters, points are taken at intervals of Δx. This results in $(l_2 - l_1)/\Delta x$ points for each dimension. Let n be the dimensionality of the potential function parameters, and use RK4 to generate the dataset $T_{\mathrm{ISNR}} = ((l_2 - l_1)/\Delta x)^n$. The dataset T_{ISNR} is then integrated with the n-dimensional parameters, and the data are standardized to facilitate subsequent training. The dataset T_{ISNR} is divided into a training set and a test set with a ratio of $r_1 = 0.8$. The trained NN model is saved for the following prediction.

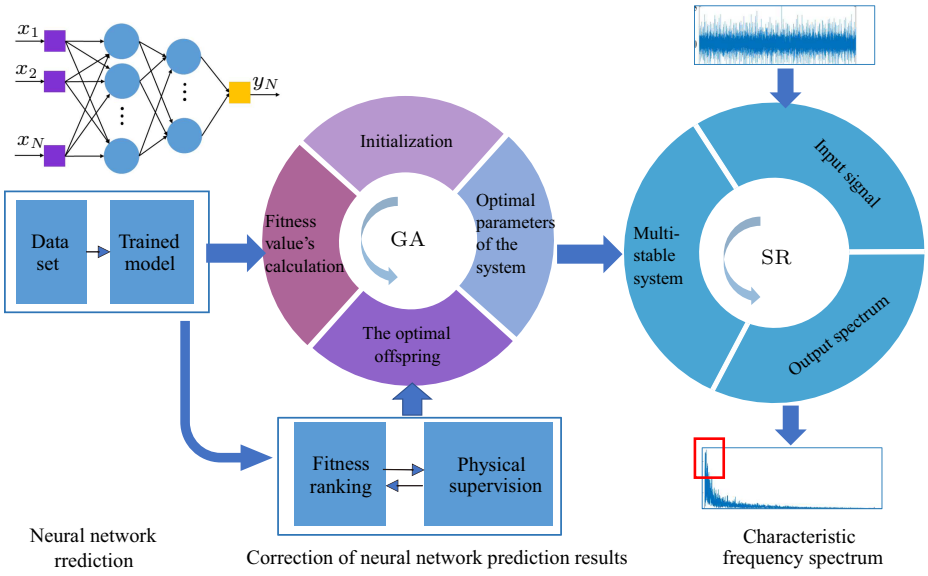


Fig. 4. ASR-PSNN process flow diagram.

The accuracy of the NN model maybe not so good that deviates from the results calculated by RK4, when the input data falls outside the range of the training samples or the training data is not enough. Such deviation may send an incorrect information to the iteration process, and the optimization process fails. To suppress the influence of prediction errors from the NN model, a physical supervision method for secondary validation is introduced to correct the results, as shown in Fig. 5. This represents the second difference from the traditional ASR. In GA, high-fitness individuals need to be retained as part of the next generation population. In the process of predicting the fitness values of the offspring population using an NN, a retention rate r is set, such that the top $P \times r$ individuals with the highest fitness are selected and preserved as X^{sub} (top performers). Subsequently, the chromosomes corresponding to these X^{sub} individuals are decoded, individuals are decoded. As the physical supervision, the RK4 method is employed to compute the fitness values of top performer individuals X^{sub} and then re-ranked when the order does not coincide with those from NN model. This secondary verification serves to decrease the deviation from error in the NN predictions, thereby ensures the accurate ranking of X^{sub} and guaranteeing the preservation of the elite individuals for the subsequent generation. The detailed steps are as follows.

Prepare: Define the ranges for a, b, c, d as $[l_1, l_2]$ with an interval of Δx. Use the RK4 results to generate NN dataset T_{ISNR}, which consists of the ISNR values corresponding to the different parameter combinations. Divide T_{ISNR} into a training set and a test set. Use training set to train the NN and save the trained model as f_{NN}.

Step 1 Initialization of the GA: Determine the population size N, number of generations G, crossover probability p_{C}, and mutation probability p_{m}, and initialize the population P_0.

Step 2 Fitness value (ISNR) calculation: Decode the individuals X_0 ($X_0 = \{x_1, x_2, \ldots, x_{\mathrm{N}}\}$) within the initial population P_0. Input the decoded potential function parameter values into the NN model f_{NN} to obtain the predicted fitness values $F(X_0)$. These predicted values $F(X_0) = f_{\mathrm{NN}}(X_0)$ serve as the fitness scores for each individual.

Step 3 GA evolution: Perform selection, crossover, and mutation operations on each individual in the parent population P_t (where $t \in [1, G]$) to generate a new offspring population P_{t+1}.

Step 4 Fitness evaluation and update: Evaluate the fitness of the evolved population P_{t+1}, rank the individuals X_{t+1} based

on their fitness values $F(X_{t+1})$, and retain the individuals X_{t+1} with the top ISNR values using a retention rate r. Record the selected individuals X_{t+1}^{sub} and their corresponding fitness values $F(X_{t+1}^{\text{sub}})$ as a subset of NN-predicted results, awaiting secondary verification.

Step 5 Physical supervision of the optimal individual: Sort the individuals X_{t+1}^{sub} by fitness values $F(X_{t+1}^{\text{sub}})$ in descending order. Decode the ranked individuals to obtain their potential function coefficients, substitute these parameters into the physical model to recalculate ISNR. Retain the individual x_{t+1}^{best} with the highest ISNR as the optimal solution in the new population.

Step 6 Termination condition check: Verify if the predetermined generation G is reached or if fitness values $F(X_t)$ show no significant improvement. If neither condition is met, retain the optimal individual and return to Step 4 for the next round of evolution. If the conditions are met, terminate the process.

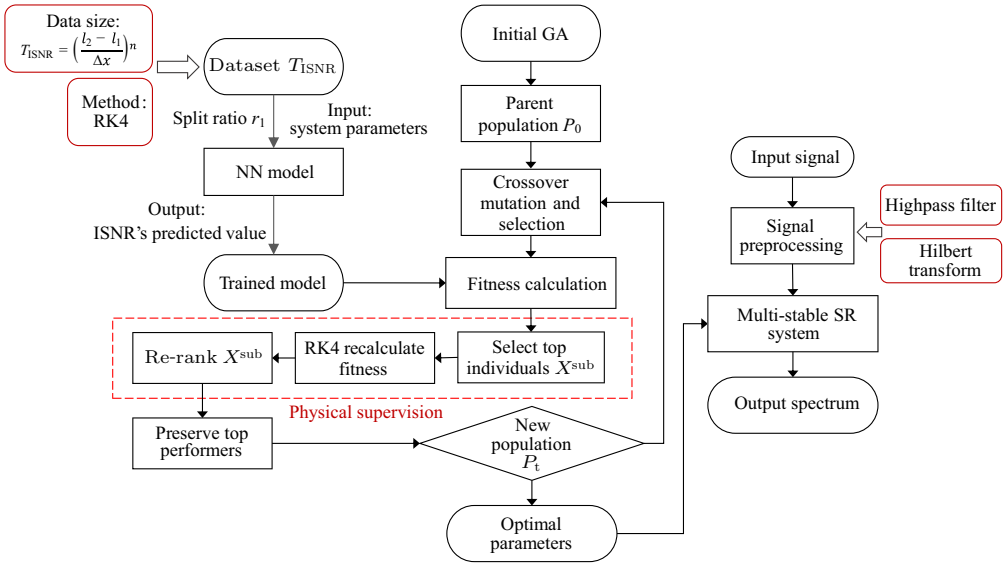


Fig. 5. ASR-PSNN program flowchart.

Algorithm ASR-PSNN algorithm

Prepare: Define the ranges for a, b, c, and d as $[l_1, l_2]$ with an interval of Δx. Use the RK4 results to generate NN dataset T_{ISNR}, and divide T_{ISNR} into a training set and a test set. Train the NN model and save it as f_{NN}.

Input: The NN trained model f_{NN}, signal awaiting detection

Output: The ASR-PSNN solution

1: Set the GA parameters N, G, p_{c}, p_{m}, and r, initialize population P_0

2: **for** $t = 1, 2, 3, \ldots, G$

3: Decode individuals X_t get the fitness value:

$$F(X_t) = f_{\text{NN}}(X_t)$$

4: Update population P_t by selection, crossover, and mutation operations:

$$P_{t+1} \leftarrow P_t$$

5: Evaluate the fitness $F(X_{t+1}) = f_{\text{NN}}(X_{t+1})$, Sort the individuals in X_{t+1} based on $F(X_{t+1})$, and retain the top $r = 0.1$ of them. Record the subset as X_{t+1}^{sub} and $F(X_{t+1}^{\text{sub}})$

6: Recalculate ISNR of subset by the physical model and retain the highest x_{t+1}^{best}

7: Condition check, if G or $F(X_t)$ reached, stop

8: **return** results

4. Numerical simulation and experiment

4.1. Small parameter input signals simulation using ASR-PSNN

In this section, small parameter signal simulations are used to verify the effectiveness of the proposed method. Let the input signal be $s(t) = A\cos(2\pi f_{\text{o}} t)$ and $N(t) = \sqrt{2D}\delta(t)$, where the amplitude of the input signal is $A = 0.1$, the characteristic frequency is $f_{\text{o}} = 0.02$ Hz. The sampling frequency is set to $f_{\text{s}} = 5$ Hz, and the number of sampling points is $N = 2000$. The range of the potential function parameters is set to [0.001, 5], and according to Subsection 3.1, the length of the sub-encoded string is $n_i = 13$ ($i = 1, 2, 3, 4$), meaning the binary encoding length for the four parameters of the potential function is 52 bits. The parameters of the GA are initialized as listed in Table 1.

Table 1. The GA parameters.

Population size	Maximum number of generations	Tournament selection	Crossover probability	Mutation probability
100	160	4	0.7	0.05

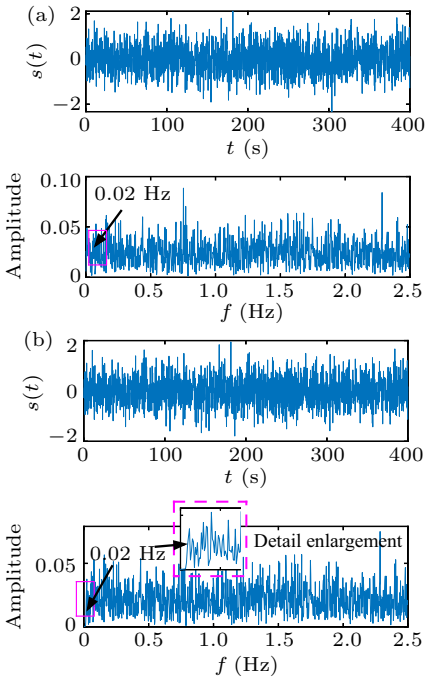


Fig. 6. Time–frequency diagram of simulated signal (a) after adding white noise and (b) after bandpass filtering.

Set the training set ratio to 0.8, and input the training set into the network to obtain the trained NN model, which will be used for subsequent ISNR value prediction. The time–domain and frequency–domain diagrams of the signal $s(t)$ with added white noise are shown in Fig. 6. It can be observed that the characteristic signal frequency f_o cannot be identified in either the time or frequency domain, with the ISNR being -26.1816 dB. To attenuate noise outside the frequency band of interest, a band filter was applied. This process isolates the frequency components around the characteristic frequency f_o, making it more distinguishable and improving the overall signal quality. After filtering, the ISNR improves to -24.1782 dB. After initializing the potential function parameters, the signal and potential function parameters were optimized using ASR-PSNN, yielding the following parameters: $a = 0.8752$, $b = 1.000$, $c = 0.1258$, $d = 0.5004$. At this point, the ISNR value is 4.974 dB. The simulation results of the small parameter input signal are shown in Fig. 7, where a distinct peak can be observed at 0.02 Hz in the output signal spectrum. The code runtime decreased from 23 s to 10 s compared to the traditional ASR method, demonstrating that the ASR-PSNN method is effective in detecting small-parameter signals embedded in Gaussian white noise. Figure 8 illustrates the iterative results and spectrum obtained using the ASR-NN method without physical supervision. The ISNR predicted values exhibit a considerable deviation from the theoretical values, and the final optimized system parameters fail to induce a satisfactory SR phenomenon, emphasizing the importance of physical supervision for accurate system parameter optimization and reliable signal detection.

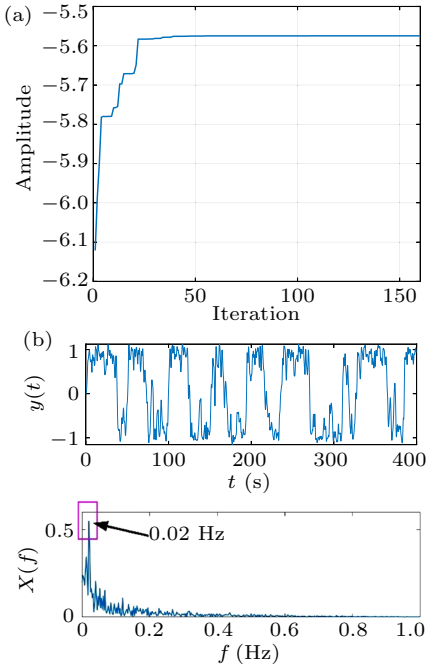


Fig. 7. ASR-PSNN result diagram of simulated signal (a) iteration curve and (b) output time–frequency.

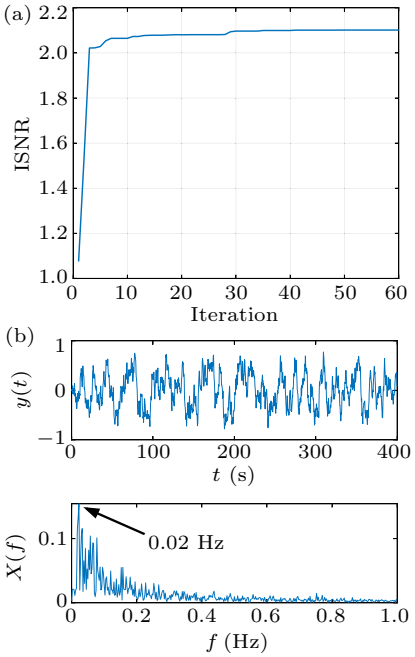


Fig. 8. ASR-NN result diagram of simulated signal (a) iteration curve and (b) output time–frequency.

4.2. Detection of outer ring fault in bearings using ASR-PSNN

4.2.1. Test bench and bearing information

To verify the feasibility of the ASR-PSNN method in engineering applications, this section uses data from the experimental platform provided by Case Western Reserve University (CWRU).

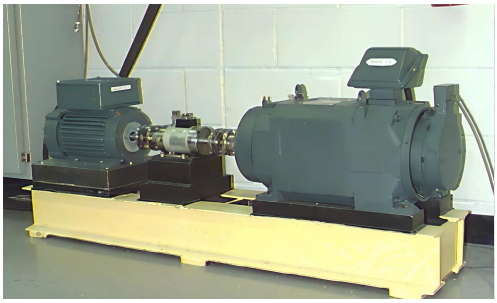


Fig. 9. CWRU test bench.

The experimental platform, as shown in Fig. 9, consists of a 1.5-kW motor (on the left), a torque sensor (in the center), a power meter (on the right), and a control electronic device (not shown in the figure).

The outer ring fault signal of the SKF6205 bearing on the drive end of the test bench is selected as the large parameter input signal. The sampling frequency is 12 kHz, the bearing speed is 1797 r/min, and the motor load is 0. The bearing specifications are listed in the table below.

During the operation of the rolling bearing, the outer ring of the bearing remains stationary, while the inner ring rotates around the axis. By substituting the rotational speed $n = 1797$ r/min into the formula for calculating the outer ring fault characteristic frequency of the bearing, the characteristic frequency is found to be $f_o = 107.36$ Hz.

$$f_o = \frac{n}{2\times 60}\left(1 - \frac{d\cos\alpha}{D_m}\right). \tag{13}$$

Table 2. Schematic diagram of the GA with operator selection.

Inner ring diameter r_1 (mm)	Outer ring diameter r_2 (mm)	Bearing contact angle α (°)	Rolling element diameter d (mm)	Pitch diameter D_m (mm)	Number of rolling elements Z
25	52	0	7.94	39.04	9

4.2.2. Detection of outer ring fault signals in bearings

Unlike small parameter SR, some signal processing is required before applying the bearing fault signal to the SR system.

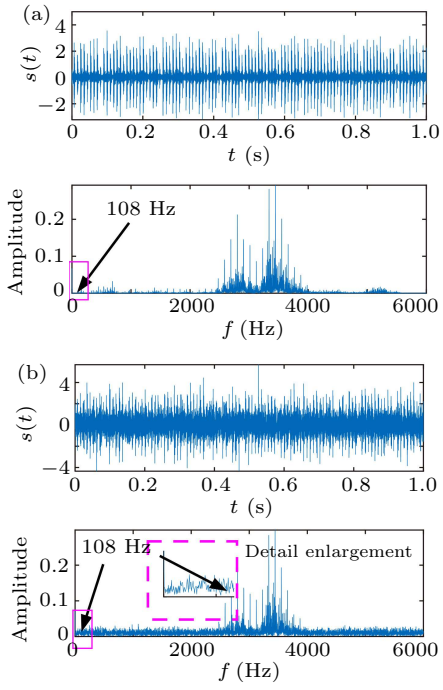


Fig. 10. Time–frequency diagram of the bearing outer ring input signal (a) without white noise and (b) with white noise.

Figure 10(a) shows the time–domain and frequency-domain plots of the experimentally collected signal for an outer ring fault in the bearing. It can be observed that there is significant high-frequency interference in the signal spectrum, with the ISNR at −44.0585 dB. To simulate the noise conditions in practical scenarios, Gaussian white noise $N(t) = \sqrt{2D}\delta(t)$ was artificially added. Figure 10(b) illustrates the signal after the addition of Gaussian white noise.

To improve the accuracy of feature extraction, appropriate signal preprocessing is required for the experimental signal $s(t)$. The bearing fault signals collected in experiments or from field measurements are typically modulated signals.[35] In this study, the experimental signal with an outer ring fault frequency is found to be very weak after modulation, which adversely affects fault feature extraction. The prerequisite for bearing fault diagnosis is to extract the fault characteristic frequency from the modulated signal, which requires demodulation of the experimental signal. In rolling bearing diagnosis, the Hilbert transform is commonly used to demodulate vibration signals,[36] while band-pass filtering can attenuate frequency components outside the passband, thereby reducing part of the noise. Mathematically, the Hilbert transform of a real signal $s(t)$ is essentially the output $\hat{s}(t)$ of the linear time-invariant system with an impulse response of $1/(\pi t)$, that is

$$\begin{aligned}\hat{s}(t) &= H[s(t)] \\ &= s(t) * (1/\pi t) = \frac{1}{\pi}\int_{-\infty}^{\infty}\frac{s(\tau)}{t-\tau}\,\mathrm{d}\tau.\end{aligned} \tag{14}$$

The signals $\hat{s}(t)$ and $s(t)$, form the analytic signal $z(t) = s(t) + \hat{s}(t)$. Consequently, the envelope of the real signal $s(t)$

can be obtained as

$$\text{Envelope}\,(t) = \sqrt{s(t)^2 + \hat{s}(t)^2}$$

(see Fig. 11). By further analyzing the envelope signal, the fault characteristic frequency can be extracted.

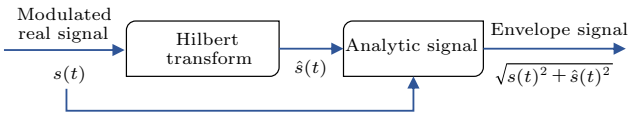


Fig. 11. Principle of the Hilbert transform.

Figure 12(a) shows the time-domain and frequency-domain plots of the signal after applying the Hilbert transform. As seen in the figures, the envelope provides a clearer representation of the signal's amplitude modulation, and the frequency-domain plot reveals reduced noise interference after the transformation. The results after applying bandpass filtering to the envelope signal are shown in Fig. 12(b), where the high-amplitude DC component in the spectrum is removed, further focusing the vibration signal within the passband.

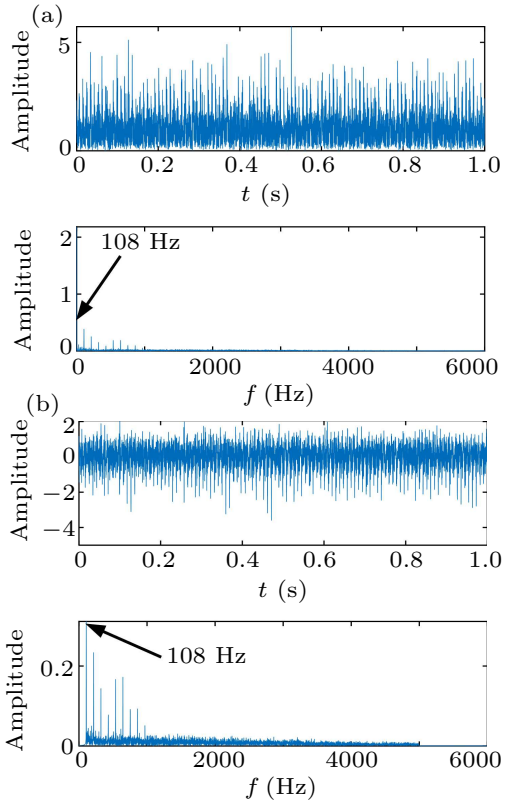


Fig. 12. Time–frequency diagram of the bearing outer ring input signal (a) after the Hilbert transform and (b) after band-pass filtering.

Subsequent to the signal preprocessing, the vibration signal requires further scale transformation. Specifically, the amplitude of the envelope signal is amplified to ensure compatibility with higher-frequency signal, thereby facilitating the occurrence of stochastic resonance. Based on the scaling theory from Section 2, a scaling factor $m = 1000$, is introduced to perform an equivalent transformation on the SR model for the large parameter input signal. The amplitude of the input signal and the noise intensity D are amplified by a factor of m. The sampling frequency is set to $f_s = 12$ kHz, and the number of sampling points is set to $N = 12000$. The range of the potential function parameters a, b, c, d is set to [0.001,5], and these parameters also need to be amplified by a factor of m. Similarly, the length of the sub-encoded string is calculated as $n_i = 13$ $(i = 1,2,3,4)$, resulting in a binary encoding length of 52 bits for the four parameters of the potential function. The remaining process is similar to that in Subsection 4.1. The higher-frequency signal and the potential function parameters optimized by are input into the SR system, and the resulting output is as shown. As observed from the evolution graph of the GA, convergence is achieved, with the code running time decreasing from 280 s to 32 s. Furthermore, the output spectrum in Fig. 13 exhibits distinct peaks at 108 Hz, demonstrating the effectiveness of this method in detecting the characteristic frequency of large parameter signals. After optimization, the system parameters achieve optimal matching with the signal and noise intensity, resulting in an improvement of the ISNR to −0.1890 dB.

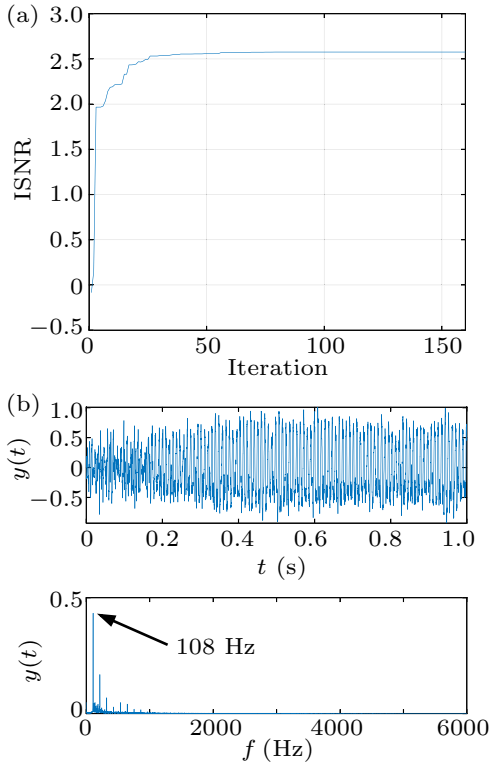


Fig. 13. ASR-PSNN result diagram of the bearing outer ring input signal (a) iteration curve and (b) output time–frequency.

Figure 14 presents the iterative results and the spectrum obtained using the ASR-NN method. As shown in the figure, due to the failure to achieve optimal parameter matching, the amplitude of the characteristic frequency in the spectrum is much lower than that in Fig. 13, and the results show a low ISNR level, preventing the effective fault identification.

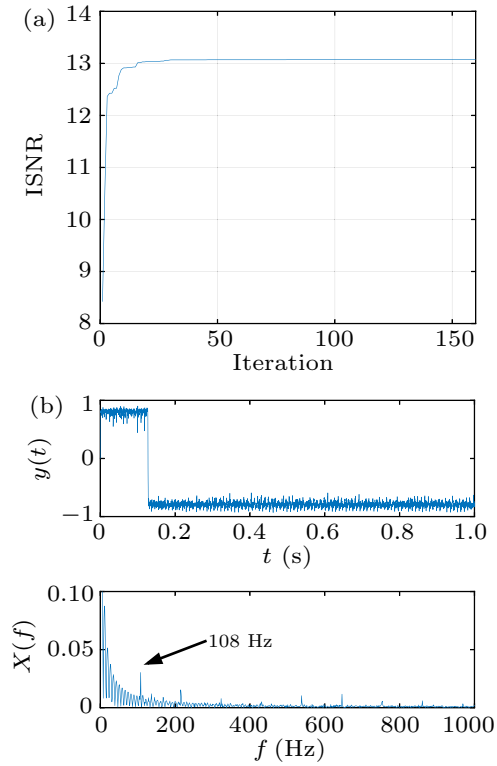


Fig. 14. ASR-NN result diagram of the bearing outer ring input signal (a) iteration curve and (b) output time–frequency.

4.3. Discussion

From the two case studied above, it can be observed that compared to traditional ASR methods, the ASR-PSNN approach significantly reduces computational costs and enhances code efficiency by replacing numerical computation steps in the iterative process with a neural network (NN). This advantage becomes particularly evident when dealing with computationally intensive tasks.

Secondly, the application of physical supervision compensates for the shortcomings of NN predictions, ensuring the integration of ASR and NN even in scenarios where a large amount of training data is not available to support NN prediction accuracy. This enables the method to achieve both high speed and sufficient accuracy.

In summary, the ASR-PSNN method proves to be effective in practical applications for complex computational tasks in fault signal detection, providing a fast and accurate detection solution. However, certain limitations remain when dealing with tasks that demand extremely high precision. In the future, further research can be conducted on small-sample NN prediction to reduce initial training costs while improving the prediction accuracy of the neural network.

5. Conclusion

This paper presents an efficient and practical detection method, ASR-PSNN, which leverages an SR system with a multi-stable potential function to enable the effective detection of both small and large parameter input signals. First, the multi-stable potential function was analyzed, and a set of different potential function parameters could change the number of stable states. Second, the improved signal-to-noise ratio (ISNR) was used as the fitness function of the optimization algorithm, making it more effective in detecting the characteristic frequency of large parameter signals. The traditional fitness value calculation was replaced by predictions from the trained NN model, which improves the solving speed. Additionally, a secondary correction of the best individual predicted by physical supervision in each generation was introduced, ensuring ASR algorithm convergence and solution accuracy. This constitutes the proposed ASR-PSNN method. Finally, the model was applied to detect the characteristic frequency of a small parameter simulation signal with a frequency of 0.02 Hz and the experimental bearing outer ring fault signal with a theoretical characteristic frequency of 107.36 Hz. The experimental results show that the proposed method is feasible for characteristic frequency detection.

While the ASR-PSNN method offers promising results, several areas for further improvement were identified. Future research could focus on optimizing NN training to reduce costs and improve prediction accuracy, particularly for scenarios with limited data. Additionally, the application of higher stable states in SR systems warrants further investigation to enhance adaptability in more complex environments. The integration of physical supervision into neural networks also highlights potential for reducing computational demands, suggesting broader applicability of the method in other domains.

In summary, ASR-PSNN provides a novel and efficient approach to signal detection, addressing key challenges in computational efficiency and detection accuracy. With further refinement, this method could find wide-ranging applications in various fields requiring advanced signal analysis.

References

[1] Benzi R, Sutera A and Vulpiani A 1981 *J. Phys. A: Math. Gen.* **14** L453
[2] Mantegna R N and Spagnolo B 1996 *Phys. Rev. Lett.* **76** 563
[3] Van den Broeck C, Parrondo J M R and Toral R 1994 *Phys. Rev. Lett.* **73** 3395
[4] Li D X, Xu W, Yue X L and Lei Y M 2012 *Nonlinear Dyn.* **70** 2237
[5] Anishchenko V S, Neiman A B, Moss F and Shimansky-Geier L 1999 *Phys. Usp.* **42** 7
[6] McDonnell M D and Abbott D 2009 *PLoS Comput. Biol.* **5** e1000348
[7] Palabas T, Torres J J, Perc M and Uzuntarla M 2023 *Chaos, Solitons and Fractals* **168** 113140
[8] He F and Yang Y 2021 *Neuroscience* **458** 213
[9] Förster A, Guderian A, Zeyer K P, Dechert G and Schneider F W 1996 *Int. J. Neur. Syst.* **7** 385
[10] Leonard D S and Reichl L E 1994 *Phys. Rev. E* **49** 1734
[11] Lu Z Q, Chen L Q, Brennan M J, Yang T J, Ding H and Liu Z G 2016 *J. Sound Vib.* **370** 221
[12] Dykman M I, Luchinsky D G, Mannella R, McClintock P V E, Stein N D and Stocks N G 1995 *Il Nuovo Cimento D* **17** 661
[13] Lindner B and Schimansky-Geier L 2000 *Phys. Rev. E* **61** 6103
[14] Liu Y J, Wang F Z, Liu L and Zhu Y M 2019 *Eur. Phys. J. B* **92** 168
[15] Liao Z Q, Ma K J, Shamim Sarker M, Yamahara H, Seki M and Tabata H 2022 *Results Phys.* **42** 105968

[16] Gong X L, Xu P F, Liu D and Zhou B L 2023 *Chaos, Solitons and Fractals* **172** 113534
[17] Mitaim S and Kosko B 1998 *Proc. IEEE* **86** 2152
[18] Liu X L, Liu H G, Yang J H, Litak G, Cheng G and Han S 2017 *Mech. Syst. Signal Process.* **96** 58
[19] Lei Y G, Han D, Lin J and He Z J 2013 *Mech. Syst. Signal Process.* **38** 113
[20] Li J M, Chen X F and He Z J 2013 *Mech. Syst. Signal Process.* **36** 240
[21] Hu N Q, Chen M and Wen X S 2003 *Mech. Syst. Signal Process.* **17** 883
[22] Guo W, Zhou Z M, Chen C and Li X 2017 *Microelectron. Reliab.* **75** 239
[23] Li J M, Zhang J F, Li M and Zhang Y G 2019 *Mech. Syst. Signal Process.* **114** 128
[24] Jin Y F, Wang H T, Xu P F and Xie W X 2023 *Probab. Eng. Mech.* **72** 103418
[25] Jin Y F, Wang H T and Zhang L L 2024 *Chin. Phys. B* **33** 010501
[26] He L F, Liu Q L and Zhang T Q 2022 *Chin. Phys. B* **31** 070503
[27] McNamara B and Wiesenfeld K 1989 *Phys. Rev. A* **39** 4854
[28] Gang H, Qing G R, Gong D C and Weng X D 1991 *Phys. Rev. A* **44** 6414
[29] Dykman M I, Luchinsky D G, Mannella R, McClintock P V E, Stein N D and Stocks N G 1993 *J. Stat. Phys.* **70** 463
[30] Huang D W, Yang J H, Zhang J L and Liu H G 2017 *Proc. Inst. Mech. Eng. C* **231** 3964
[31] Michalewicz Z and Schoenauer M 1996 *Evol. Comput.* **4** 1
[32] Bhoskar M S T, Kulkarni M R O K, Kulkarni M R N K, Patekar M S S L, Kakandikar G M and Nandedkar V M 2015 *Mater. Today: Proc.* **2** 2624
[33] Katoch S, Chauhan S S and Kumar V 2021 *Multimed. Tools Appl.* **80** 8091
[34] Wang J, Zhang Q, Liang N, Zhang Y Z and Xu G H 2010 *Journal of Xi'an Jiaotong University* **44** 32
[35] Yang J H and Zhou D J 2020 *Re-scaled Resonance Theory and Application in Fault Diagnosis* (Beijing: Science Press) p. 76
[36] Feldman M 2011 *Mech. Syst. Signal Process.* **25** 735